David J. Unger*

Path-dependent J-integral evaluations around an elliptical hole for large deformation theory

DOI 10.1515/jmbm-2016-0008

Abstract: An exact expression is obtained for a path-dependent J-integral for finite strains of an elliptical hole subject to remote tensile tractions under the Tresca deformation theory for a thin plate composed of non-work hardening material. Possible applications include an analytical resistance curve for the initial stage of crack propagation due to crack tip blunting.

Keywords: nonlinear crack problem; path-dependent integral; *R*-curve; resistance curve; Tresca yield condition.

1 Introduction

Many finite element schemes of simulated crack problems have demonstrated the path dependence of the J-integral [1] as a result of non-proportional loading. This type of behavior may occur because of finite deformations of an elastic-plastic material [2] or through the use of flow theories of plasticity with small strains in elastic-plastic analyses [3, 4]. In general [5], any nonlinear elastic material for finite deformations will exhibit path-dependent J-integrals for crack problems.

However, no exact mathematical evaluation of a path-dependent integral has been derived to date from which one may draw more general conclusions about how parameters affect these integrals. Here, exact expressions are derived for J-integrals of finite deformations of a nonlinear elastic material satisfying the Tresca yield condition. A traction-free elliptical hole subject to remote tensile tractions for a non-strain hardening material is used to represent a crack under plane stress loading conditions.

The closed J-integral, as defined in [1] for a plane problem, is

$$J_\Gamma=\int_\Gamma W dy-\mathbf{T}\cdot\frac{\partial\mathbf{u}}{\partial x}ds=0, \tag{1}$$

where W is the strain-energy density, x and y are Cartesian coordinates, and Γ is the path of integration, on which ds is the differential arc length, $\mathbf{u}$ is the displacement, and $\mathbf{T}$ is the traction. For cases where the integral becomes path-dependent, its evaluation around Γ is no longer zero as indicated in Eq. (1).

In [6, 7], an explicit analytical solution for an elliptic hole in a non-work hardening material was derived. In [8], the analogous problem was solved for large deformations. A pair of superposed coordinates was defined in [8], where the uppercase letters represent the initial undeformed state of the material and the lowercase letters represent the deformed configuration, as indicated in Figure 1.

The natural or logarithmic strain rate was determined there as

$$\dot{\varepsilon}_{\alpha\alpha}^{\log}=\frac{v_0}{\rho+F(\alpha)}=\frac{v_0}{R+F(\alpha)+v_0\tau}, \tag{2}$$

where

$$F(\alpha)=\frac{a^2b^2}{(a^2\cos^2\alpha+b^2\sin^2\alpha)^{3/2}},\quad u_0=v_0\tau,\ \rho=R+u_0. \tag{3}$$

In Eqs. (2) and (3), R is the distance along a normal or slip line from the elliptical hole to a particular point in the undeformed configuration (Figure 1). The angle α measures the inclination of an arbitrary slip line orthonormal to the elliptical boundary in both the (X, Y) and (x, y) systems. The magnitude of displacement u_0 is uniform for all slip lines and acts in the direction of the slip line. The parameter v_0 is the constant rate of displacement with respect to the loading parameter τ.

The nonlinear strain energy density may be determined from the following integral, assuming the material is nonlinear elastic.

$$W=2k\int_0^\tau\dot{\varepsilon}_{\alpha\alpha}^{\log}d\tau=2k\int_0^\tau\frac{v_0\,d\tau}{R+F(\alpha)+v_0\tau}=2k\ln\left(1+\frac{v_0\tau}{R+F(\alpha)}\right)=2k\ln\left(1+\frac{u_0}{R+F(\alpha)}\right), \tag{4}$$

where k is the yield strength in pure shear. No other strain component contributes to W. The coordinate Y in differential form in the initial configuration notation [8] is

***Corresponding author: David J. Unger,** Department of Mechanical and Civil Engineering, University of Evansville, 1800 Lincoln Avenue, Evansville, IN 47722, USA, e-mail: du2@evansville.edu

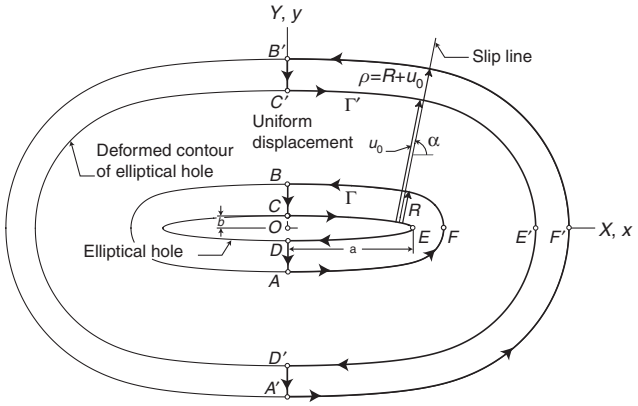

Figure 1: Path of integration in both the initial coordinates (X, Y) and in the deformed state (x, y).

$$dY=\sin\alpha\, dR+(R+F(\alpha))\cos\alpha\, d\alpha. \tag{5}$$

The J-integral (1) is now divided into two distinct parts

$$J_\Gamma^{(1)}=\int_\Gamma W dY,\quad J_\Gamma^{(2)}=-\int_\Gamma \mathbf{T}\cdot\frac{\partial\mathbf{u}}{\partial X}dS. \tag{6}$$

As in the case of small deformation theory [7], the traction $\mathbf{T}$ and $\partial\mathbf{u}/\partial X$ vectors remain orthogonal to one another during deformation and, consequently, they provide no contribution to $J_\Gamma^{(2)}$. Because of this, the only nontrivial component of J_Γ reduces to that of the first integral of (6), i.e. $J_\Gamma^{(1)}$.

Now there are two distinct paths to be analyzed separately for $J_\Gamma^{(1)}$, as shown in Figure 1. One particular class is along the Y-axis, i.e. BC ($\alpha=\pi/2$) and DA ($\alpha=-\pi/2$), such that

$$J^{(1)}\Big|_{\alpha=\pm\frac{\pi}{2}}=2k\int_{R_1}^{R_2}\ln\left(1+\frac{u_0}{R+a^2/b}\right)dR. \tag{7}$$

This integral has the elementary solution

$$\begin{aligned}J^{(1)}\Big|_{\alpha=\pm\frac{\pi}{2}}=&\frac{2k}{b}\left\{bu_0\ln\left[\frac{a^2+b(u_0+R_2)}{a^2+b(u_0+R_1)}\right]\right.\\&+\left(a^2+bR_2\right)\ln\left(1+\frac{bu_0}{a^2+bR_2}\right)\\&\left.-\left(a^2+bR_1\right)\ln\left(1+\frac{bu_0}{a^2+bR_1}\right)\right\}.\end{aligned} \tag{8}$$

Provided one keeps the paths BC and DA of equal length, the two contributions from Eq. (8) cancel each other over the closed path Γ and consequently do not contribute to the path dependence of $J_\Gamma^{(1)}$.

A much more challenging integral to evaluate analytically occurs along path AFB of Figure 1, whose form for a constant but arbitrary value of R is

$$\begin{aligned}J=&J^{(1)}\Big|_{R=\text{const}}\\=&2k\int_{-\pi/2}^{\pi/2}\ln\left(1+\frac{u_0}{R+F(\alpha)}\right)\Big(R+F(\alpha)\Big)\cos\alpha\, d\alpha,\end{aligned} \tag{9}$$

where $F(\alpha)$ is given in Eq. (3). Initial attempts at evaluating this integral directly, using a symbolic mathematical computer program, failed to produce meaningful results. Nevertheless, under the specified sequence of transformation of variables to follow, an exact expression can be found.

Making the following substitutions in Eq. (9), where several functions are identified as standard Jacobian elliptic functions [9],

$$\begin{aligned}&\alpha=\text{am}(z\backslash m)\rightarrow d\alpha=\text{dn}\, z\, dz\\&\cos\alpha=\cos(\text{am}(z\backslash m))=\text{cn}\, z,\ m=1-(b/a)^2,\\&\sin\alpha=\sin(\text{am}(z\backslash m))=\text{sn}\, z,\ F(\alpha)=(b^2/a)\ \text{nd}^3 z,\end{aligned} \tag{10}$$

one obtains

$$\begin{aligned}J=&2k\int_{-K(m)}^{K(m)}\ln\left(1+\frac{u_0}{R+(b^2/a)\ \text{nd}^3 z}\right)\\&\times(R+(b^2/a)\ \text{nd}^3 z)\ \text{dn}\, z\ \text{cn}\, z\, dz,\end{aligned} \tag{11}$$

where the modulus of the elliptic functions is m. The complete elliptic integral of the first kind that is found in the limits of integration in Eq. (11) is defined by

$$K(m)=\int_0^{\pi/2}\frac{d\theta}{\sqrt{1-m\sin^2\theta}}. \tag{12}$$

One should be aware that a common alternative representation for parameter m is k^2 as in [10]. If this notation is employed, then it also carries over to the related Jacobian elliptic functions modulus in (10).

An additional transform of z to ϕ in Eq. (11) of the form

$$\begin{aligned}\phi=&\int\text{cn}\, z\, dz\\=&\frac{1}{\sqrt{m}}\cos^{-1}(\text{dn}\, z)\rightarrow\text{dn}\, z=\cos\sqrt{m}\,\phi,\end{aligned} \tag{13}$$

will simplify this integral to

$$\begin{aligned}J=&4k\int_0^{\cos^{-1}(b/\sqrt{a^2-b^2})}\ln\left(1+\frac{u_0}{R+(b^2/a)\ \sec^3\sqrt{m}\phi}\right)\\&\times(R+(b^2/a)\sec^3\sqrt{m}\phi)\cos\sqrt{m}\,\phi\, d\phi,\end{aligned} \tag{14}$$

where an additional factor of 2 ahead of this integral accounts for the symmetry of the integrand with respect to the X-axis that was used.

Further, use of the transformation

$$\phi=(1/\sqrt{m})\cos^{-1}\lambda, \tag{15}$$

reduces the integral in Eq. (14) to

$$J=\frac{4k}{\sqrt{a^2-b^2}}\int_{b/a}^{1}\ln\left(1+\frac{u_0 a\lambda^3}{Ra\lambda^3+b^2}\right)\times\frac{(Ra\lambda^3+b^2)d\lambda}{\lambda^2\sqrt{1-\lambda^2}}. \tag{16}$$

The following and the last of the transformations (see [11]) reduces the algebraic function outside of the argument of the log function in Eq. (16) to a rational function of t while leaving the argument of the log a rational function, albeit of a higher order

$$\lambda=\frac{2t}{1+t^2}. \tag{17}$$

Consequently, upon substitution of λ in Eq. (16), one finds that

$$J=\frac{2kb^2}{\sqrt{a^2-b^2}}\int_{\frac{a}{b}-\frac{\sqrt{a^2-b^2}}{b}}^{1}\left(1+\frac{1}{t^2}+\frac{8(R_0)^3 t}{(1+t^2)^2}\right)\times\ln\left(\frac{1+3t^2+8(D_0)^3t^3+3t^4+t^6}{1+3t^2+8(R_0)^3t^3+3t^4+t^6}\right)dt, \tag{18}$$

where various parameters appearing in Eq. (18) are defined by

$$R_0=\left(\frac{aR}{b^2}\right)^{1/3},\ D_0=(aU_0/b^2)^{1/3},\ U_0=\rho=R+u_0. \tag{19}$$

Symbolic mathematical computer programs can generally integrate a logarithm of the linear function of the integration variable multiplied by a rational function of the same variable outside the argument. Similarly, standard integral tables such as [12] typically list entries having the same mathematical construct.

By factoring the numerator and denominator of the argument of the log function in Eq. (18), a general representation of the integral assumes the following form

$$J=\frac{2kb^2}{\sqrt{a^2-b^2}}\int_{\frac{a}{b}-\frac{\sqrt{a^2-b^2}}{b}}^{1}\left(1+\frac{1}{t^2}+\frac{8(R_0)^3 t}{(1+t^2)^2}\right)\times\ln\left[\frac{\prod_{n=1}^{6}(t-t_n)}{\prod_{n=7}^{12}(t-t_n)}\right]dt, \tag{20}$$

where t_n represents a root of either the numerator or denominator of the argument of the log function. Subsequently, using standard properties of logarithms, one can expand the integrand of Eq. (20) into 12 distinct integrals, all of which have a linear dependence of t in the argument of the log function. Hardy [13] provides criteria from which one can predict that the integral in Eq. (20) should contain only elementary transcendental functions and rational functions in its evaluation. This surprising prediction proved true.

Although both the numerator and denominator of the argument of the log function in Eq. (18) are of sixth order, exact roots of these reduced polynomials can be readily found algebraically. The exact evaluation of Eq. (20) was obtained in this fashion using Mathematica® 1.0 (Wolfram Research Champaign, IL, USA); however, its length precludes the entire solution being reproduced here.

Representative behavior using the entire solution is plotted in Figure 2 for a specific value of displacement $u_0/a=0.02$. Note the symbol J_0 appearing in the figure, as a normalizing parameter, is the value of J obtained in [7] for small displacements and strains, i.e.

$$J_0=4ku_0. \tag{21}$$

For the Tresca yield condition, the yield strength in tension σ_0 is equal to twice the yield strength in shear k. The crack opening displacement δ can be defined as the change in separation between points C and C' plus D and D' of Figure 1, which is equal to $2u_0$. Therefore, Eq. (21) can be rewritten as

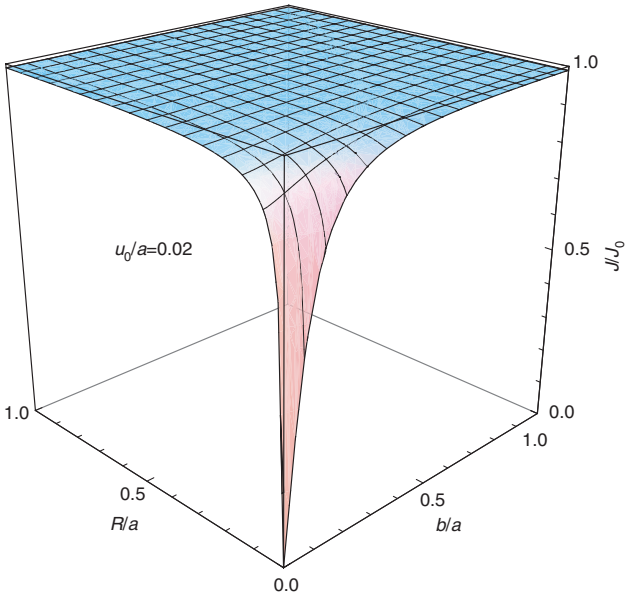

Figure 2: Normalized J-integral as a function of elliptical axes aspect ratio and normalized distance from the internal boundary.

$$J_0=\sigma_0\delta, \tag{22}$$

which is reminiscent of the form of the crack tip opening displacement δ_t, defined in [1], for the Barenblatt-Dugale model of crack tip plasticity.

A special and important case (R=0) of the complete analytical solution will now be given explicitly. Its length is considerably shorter than the general result, making it possible to present it here. This formula applies to the evaluation of the integral in Eq. (20) along a path following one half of the elliptical hole, i.e. as AFB approaches DEC in Figure 1. This path produces the smallest value of the J-integral possible for a fixed aspect ratio b/a and displacement u_0/a. It assumes the mathematical form

$$\begin{aligned}\left.\frac{J}{J_0}\right|_{R=0} &= (b/u_0)\ln\left(1+\frac{u_0 b}{a^2}\right)\\ &+\frac{2b^2}{au_0\sqrt{1-(b/a)^2}}\left\{\sqrt{1-d^2}\,\tan^{-1}\left(c\sqrt{\frac{1-d}{1+d}}\right)-3\pi/4\right.\\ &-3\tan^{-1}\left[(-a+\sqrt{a^2-b^2})/b\right]\\ &+\sqrt{1+(-1)^{1/3}d^2}\,\tan^{-1}\left(c\frac{\sqrt{1+(-1)^{1/3}d^2}}{1+(-1)^{2/3}d}\right)\\ &\left.+\sqrt{1-(-1)^{2/3}d^2}\,\tan^{-1}\left(c\frac{1+(-1)^{1/3}d}{\sqrt{1-(-1)^{2/3}d^2}}\right)\right\},\end{aligned} \tag{23}$$

where the two parameters c and d found in Eq. (23) are defined by

$$c=\frac{b-a+\sqrt{a^2-b^2}}{b+a-\sqrt{a^2-b^2}},\quad d=\left(\frac{au_0}{b^2}\right)^{1/3}. \tag{24}$$

In Figure 3, one finds relationship in Eq. (23) plotted versus the aspect ratio b/a for various values of u_0/a. One observes that as the elliptical hole geometry approaches a line crack ($b\to 0$) the J-integral evaluation approaches zero for all values of displacement.

In Figure 4, the normalized J-integral from the complete solution is plotted as a function of the normalized distance from the elliptical hole (R/a) for the range of permissible aspect ratios ($0<b/a<1$) at a fixed value of displacement u_0/a=0.02. As b approaches zero in Figure 4, the inside envelope of curves approaches the locus of the asymptotic expansion of the complete solution, i.e.

$$J\sim 4kR\,\ln\left(1+\frac{u_0}{R}\right)\ \text{as}\ b\to 0. \tag{25}$$

The limit of J in the asymptotic expansion of Eq. (25) as R goes to zero is zero.

2 Discussion

There exist no finite element analyses for large deformation crack or notch problems involving the Tresca yield condition. Should there be any in the future, the solution obtained here can serve as a benchmark for comparison.

However, if one compares how the value of the normalized J-integral changes with distance from the notch boundary in Figure 4 to the elastic-perfectly plastic data (n=0) plotted in Figure 9 of [2], the two loci qualitatively resemble one another despite several differences that exist between the two analyses.

For example, both analyses indicate that for finite deformations, the J-integral tends toward zero as the paths

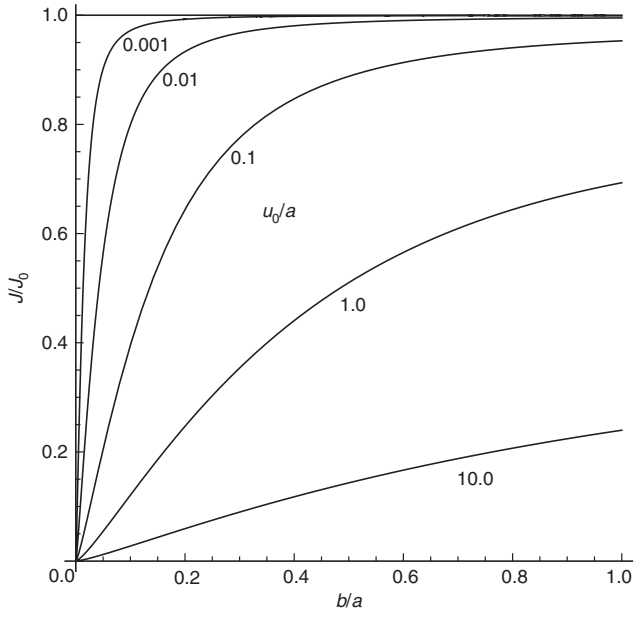

Figure 3: Normalized J-integral along the elliptical hole boundary versus axes aspect ratio and normalized displacement.

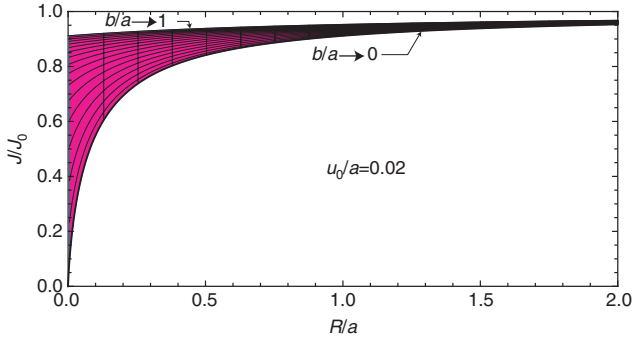

Figure 4: Envelope of normalized J-Integral values versus normalized distance from elliptical boundary at a fixed displacement.

of integration approach the notch boundary. McMeeking [2] attributes this effect due to crack tip blunting. In contrast, in an elastic-perfectly plastic analysis performed in [3] for a sharp crack, a normalized J-integral in their Figure 3 approaches a non-zero value of J as the path of integration approaches the crack tip. No blunting of the crack tip was incorporated into this particular analysis. Both analyses [2] and [3], however, use a flow theory of plasticity under the von Mises yield condition.

Lastly, it should be pointed out that for a value of b/a equal to zero, the analytical solution employed here degenerates [6, 7]. However, one may approach a line crack to any degree of accuracy desired as long as b remains finite.

For the case b=0, a statically admissible solution is proposed in [6]; however, it requires the formation of a stress discontinuity. A stress discontinuity is also encountered in the plane stress perfectly plastic analysis [14] using the von Mises yield condition for a semi-infinite line crack.

If this J-integral is interpreted as an energy dissipation rate instead of an energy release rate, then a theoretical resistance curve (R-curve) is obtained in closed form for the initial stage of crack extension due to crack tip blunting, e.g. in Eq. (25) as b→0 with $u_0=\Delta a$. Previously [15], modeling of this region was limited to relationships having the form

$$J=M\sigma_0\Delta a, \tag{26}$$

which is an offshoot of Eq. (22), where the change of crack length due to blunting Δa is approximated by $\delta/2$ [16] and M is taken as 2 [16] or higher [15]. The flow stress σ_{flow} may also be substituted into Eq. (26) in place of σ_0 in order to incorporate effects due to strain hardening [15].

References

[1] Rice, JR. *J. Appl. Mech.* 1968, 35, 379–386.
[2] McMeeking, RM. *J. Mech. Phys. Solids* 1977, 25, 357–381.
[3] Carka, D, Landis, CM. *J. Appl. Mech.* 2011, 78, 011006.
[4] Carka, D, McMeeking, RM, Landis, CM. *J. Appl. Mech.* 2012, 79, 044502.
[5] Chen, HK, Shield, RT. *Z. Agnew. Math. Phys* 1977, 28, 1–22.
[6] Unger, DJ. *Theor. Appl. Fract. Mech.* 2005, 44, 82–94.
[7] Unger, DJ. *J. Elasticity* 2008, 92, 217–226.
[8] Unger, DJ. *J. Elasticity* 2010, 99, 117–130.
[9] Abramowitz, M, Stegun, IA. *Handbook of Mathematical Functions with Formulas, Graphs and Mathematical Tables.* National Bureau of Standards, Series 55, U.S. Printing Office: Washington, DC, 1964.
[10] Byrd, PF, Friedman, MD. *Handbook of Elliptic Integrals for Engineers and Scientists*, 2nd ed., Springer-Verlag: New York, 1971.
[11] Zwillinger, D. *Handbook of Integration*. Jones and Bartlett: Boston, 1992, 145–147.
[12] Gradshteyn, IS, Ryzhik, IM. *Table of Integrals, Series, and Products.* Academic Press: Orlando, 1980.
[13] Hardy, GH. *The Integration of Functions of a Single Variable*, 2nd edn., Dover Phoenix Editions: Dover, Mineola, New York, 2005, 60–61.
[14] Hutchinson, JW. *J. Mech. Phys. Solids* 1968, 16, 337–347.
[15] ASTM Committee E 1820-1. *Standard Test Method for Measurement of Fracture Toughness*. Annual Book of ASTM Standards, Vol. 03.01. ASTM, West Conshohocken, PA, 2002, 1031–1076.
[16] Hertzberg, RW. *Deformation and Fracture Mechanics of Engineering Materials*, 4th ed., Wiley: Hoboken, NJ, 1996, 366.